Ligands docking to ORF8 by co-evolution. Could they reduce the inflammation levels induced by SARS-COV-2 infections?

short title: ORF8 co-evolutionary docking

Bello-Perez, M[+]. and Coll, J[*].
[+]Unidad Enfermedades Infecciosas. Hospital Universitario. Elche, Spain
[*]Department of Biotechnology. Centro Nacional INIA-CSIC. Madrid, Spain.
[+]Melissa Bello-Perez, orcid: 0000-0002-9212-083X
Email: melissa.bello@alu.umh.es (MB)
[*]Julio Coll, orcid: 0000-0001-8496-3493
Email: juliocollm@gmail.com (JC)
[*] Corresponding author

Abstract

The unique ORF8 is an asymmetric homodimer accessory protein of SARS-COV-2 implicated in pathogenesis by activating excesive human inflammation causing numerous deaths. There is no approved drug targeting ORF8, nor it is known whether any anti-ORF8 drugs could reduce coronavirus-induced excesive inflammation. Computationally combining ligand co-evolution of parent molecules with affinity-ranking by consensus docking, children candidates for ORF8 cavities and ligands were generated. Targeting the interface cavity with the highest affinity children scaffolds, hundreds of grandchildren were generated by specificity-toxicity controlled additional co-evolutions to predict nanoMolar affinities, unique scaffolds, high specificities and low toxicity risks. Although remaining hypothetical without experimental confirmation, these constitute a new methodological attempt to search for drug-like candidates to interfere with SARS-COV-2-dependent excessive inflammation.

Keywords: co-evolutionary docking; consensus docking; ORF8, SARS-CoV-2

Introduction

The ORF8 is one of the six viral accessory proteins of SARS-CoV-2. Dispensable for viral replication, the accessory proteins interact with the immune response, most of them playing a crucial role in the pathogenesis of human coronaviruses. ORF8 is unique among other beta-coronavirus, as the sequence identity between SARS-CoV and SARS-CoV-2 is low (~ 26 %)[1], probably to best adapt to human hosts [2]. Focused studies on SARS-CoV-2 ORF8 show an increasing trend during the last 2-years that have implicated ORF8 in many aspects of immune evasion [3, 4] and other enigmatic functions [5]. Recently, SARS-CoV-2 ORF8 has been describe as a virulence factor[5], as the infection of mice with ORF8 deleted virus and people infected with natural variants lacking the ORF8 showed a milder COVID-19 disease, due to the reduction of excesive levels of host pro-inflammatory cytokines induced after SARS-CoV-2 infection. In addition, levels of ORF8 in blood correlated with mortality in infected patients [6-8].

ORF8 shows a high number of variations [9-12] and its largest interactome suggested ORF8 implications in many different functions[13-15]. For instance, some of the effects known to be modulated by ORF8 include host endoplasmic stress [16-18], histone modification [19], SARS-CoV-2 spike S expression [20-22], inhibition of complement [23], inhibition of host interferon responses [24-27], binding to dendritic cells producer of inflammatory cytokines [28], activation of the IL17 pathway [29, 30], inhibition of antibody-dependent cellular cytotoxicity [31], and activation of pro-inflammatory storm-causing cytokines trough NLPR3 [32]. Furthermore, ORF8 covalent dimers downregulated MHC1 in host cytotoxic lymphocytes to favour viral immune evasion[33-35].

The ORF8 is an asymmetric covalent AB homodimer of 121 amino acid monomers (15 first residues of signal peptide per monomer). The core of each ORF8 monomer consists of two antiparallel β-sheets [36]. Crystallographically, two different possible dimer interfaces have ben proposed, the demonstrated covalently stabilized by a ^{20}C-^{20}C disulphide bond and the hypothetical non-covalently stabilized by the ^{73}YIDI-motif hydrophobic interactions[37-39].

ORF8 monomers, contain an Ig-like fold stabilized by intramolecular disulphides (^{25}C-^{90}C, ^{37}C-^{102}C)[37] and a highly-dynamic fold loop (hypervariable loop) flanked by its ^{61}C-^{83}C disulphide, coding for a ^{73}YIDI motif including a glycosylation site (^{78}N). The hypervariable loop has been implicated in the many host protein interactions mentioned above, capable of adapting its fold to any of those different ligands[38]. However, to our knowledge, there are no crystallographic ORF8-protein complex structures reported to date.

The ORF8 homodimer disulphide highly interdigitated interface is made up of complementary A-B amino acid surfaces implicating salt bridges (^{119}D-^{115}R and ^{115}R-^{92}E), hydrogen bonds (^{120}F-^{53}K, ^{53}K-^{24}S, ^{18}Q-^{22}L, ^{52}R-^{121}I) and many other hydrophobic interactions [36]. The predominant natural mutants of ORF8 include the L^{84}S mutation, but S^{24}L and V^{62}L additional mutations are also abundant [39, 40]. The L^{84}S mutation reduced some of the dimer interacting amino acid, including those implicated in salt bridges (i.e., ^{119}D, ^{115}R), hydrogen bonds (^{120}F, ^{53}K, ^{52}R, ^{121}I), and other interface interactions (^{98}R, ^{104}I, ^{117}V)[41].

The ORF8 is secreted into the blood of infected hosts both in N-linked glycosylated (^{78}N) [42] and unglycosylated [43] forms, inducing the highest immunogenicity among the SARS-CoV-2 proteins, specially immunodominant is its amino-terminal α-helix[44]. The ORF8 accessory protein has been proposed to modulate the recognition of viral antigens *via* antigen presenting monocytes, showing a stronger interaction of ORF8 with CD14+ monocytes using NLPR3 receptor, than with any other immune cells. The unglycosylated ORF8 binding to CD14+ monocytes causes a dysregulation of the inflammatory response characterized by elevated blood concentrations of interleukin-6, granulocyte-macrophage colony stimulating factor, and tumour necrosis factor alpha among other cytokines (cytokine storm). Some ORF8 variants (^{84}L and ^{84}S), proteins have different interaction capabilities with human CD14+ monocytes. Thus, the higher CD14+ binding by the ^{84}L variant and the milder disease outcome produced by the ^{84}S variant and its weaker binding to CD14^{+} monocytes, suggested that the ratio of these ORF8 variants may control different degrees of inflammation by modulating monocyte recognition of viral antigens depending on the host immune reactions[45].

On the other hand, it was described that ORF8 modulates the recognition of viral antigen via downregulation of MHC1. Because the down regulation of MHC1 was shown to be dimer-dependent[33-35], disruption of the dimer interface perhaps could be employed to neutralize ORF8 effects, as recently suggested[35]. Therefore, in this work, we included the exploration of the homodimer interface of SARS-CoV-2 ORF8 as a potential target for specific antiviral ligands as a first step to develop a possible therapeutic target, rather than targeting a host factor which may be essential for other physiological functions[32]. In contrast to previous computational work which only targeted the ^{20}C-^{20}C disulphide [35], an alternative strategy including blind-docking of the whole ORF8 molecule, was favoured in this work. Therefore, the best docking-cavities described here were automatically selected by the programs used, minimizing any *a priori* selection.

The present work explored the co-evolution of ORF8 / ligand pair starting from an artificial pseudoligand parent. Because of the affinity limitations of the previously proposed computationally defined ligands[35], a polyCarbon pseudoligand centered at the ORF8 molecule and widely extending in 4 directions was drawn and manually docked in PyMol to be used as initial parent to start co-evolutions (see more details in methods). The ***D**ata**W**arrior* (*DW*) ***B**uild **E**volutionary **L**ibrary* (*BEL*) algorithms[2-5] were employed here to successfully generate polyCarbon-derived children fitting the program-chosen best ORF8 interface cavities. The best affinity children-scaffolds targeting the interface cavities were then selected for further co-evolutionary refinement, seeking to increase their children affinities. *DW-BEL* co-evolutionary dockings of those new children scaffolds as parents were capable of generating large numbers of highly specific-fitting grandparent children ligands. The high computer memories required to perform such co-evolutionary searches was higher than in our previously reported work[2-5] indicating that targeting the ORF8 interface cavities had enormous steric difficulties most probably due to the strong interdigitating amino acids of its monomer faces. The generation of children molecules during co-evolution were controlled for molecular weight, hydrophobicity [6, 7, 8-11] and toxicity risks to avoid unspecificities and/or toxic molecules[46]. The most accurate **A**uto**D**ock**V**ina (ADV) program quantitatively estimated their affinities, and explore for the possibilities of whole ORF8 wide docking cavities[47].

Because of the absence of experimental data, the predicted docking-cavities and their new ligand candidates remain hypothetical. Some of the predicted results were included as **Supplementary Material** including tables with sliders. Further co-evolutions could be applied by increasing computer memories in the future because the vast chemical space limits have not been yet reached.

Computational Methods

Starting *DataWarrior "Build Evolutionary Library"* with a home-designed parent molecular pseudoligand

The *DataWarrior (DW)* updated program was downloaded (https://openmolecules.org/datawarrior/download.html) following the details for Windows as described before [46, 48].

To explore the initial cavity an star-like carbon molecule of C89H180 formula, was drawn in the ICM Molecular editor and saved as a 2D *.sdf file. It will be called here "erizo". After several trial-and-error attempts, the final erizo design contained a central carbon branched by 4 arms of 7 carbons per arm, having all carbons saturated with methyls (molecular weight 1249, logP 28.2). After drawing, the erizo was manually docked to the center of the ORF8 molecule in PyMol and saved as a *.pdb file to start *DW-BEL* co-evolutions (**Figure 1 up, red spheres** and **Figure 2 up-left**). The *DW-BEL* fits the children with flexibility around the erizo-supplied cavity, dynamically adapting its cavity to the best fit of the evolving children ligands, as visualized by the resulting images of their *.dwar files.

In this work, the fitness criteria preferences and their weight values incorporated into the *DW Build Evolutionary Library* (*DW-BEL*) for evolutionary docking (co-evolution criteria), were: minimal *DW* docking-scores (weight 4), molecular weights <= 600 g/mol (2), cLog <=4 (1) and Toxicity risk <=1 (4). The *DW* Docking-scores used the mmff94s+ force-field algorithm[49] and specially saved as *sdf files with selected options to best preserve the 2D geometry of the docked children molecules (**Table S1**). The number of runs were limited when reaching 100 Gb of computer memory.

The raw and fitted children data were saved as *.dwar files for storage of the complete co-evolution including docking-scores, chemical properties (molecular weights and LogP hydrophobicities), fitness values and cavity-children images. Before their use, the fitted children data were further filtered using a macro to exclude any remaining toxicities and/or nasty function fragment-containing children molecules (filtering for hundreds of mutagenesis, tumorigenicity, reproductive interference, irritant, and/or nasty functions) (**Supplementary Material / NTN.dwam** and **/ Nasty_functions.dwar**). The corresponding fitted children Special SD-files (*.sdf) were also saved as described in detail at **Table S1**. This saving method supplied *.sdf files maintaining the 3D protein cavity docked to children 3D conformers for visualization in PyMol (using its split_states command)[48] and/or maximal preservation of their 2D geometries for optimal consensus docking.

AutoDockVina docking program

The **A**uto**D**ock**V**ina (ADV) program written in Python vs3.8 included into a modified PyRx-098/PyRx-0.98/1.0 package[46] was used as described before. Some modifications were included here to employ a wide grid to fine-tune docking cavities, to compare with *DW-BEL* docking-scores, quantify affinities in approximated nM and generate protein / ligand 3D images[48, 50-52] (https://pyrx.sourceforge.io/).

Briefly, *.pdbqt file conversion of ORF8 and ligands[53] were made in the mmff94s (Merck) force-field. Ligands for ADV were supplied only as DW-BEL generated children in *sdf files, carefully saved as mentioned above for maximal preservation of most of their 2D geometries after docking. ADV generates many 3D conformers using the rotatable bonds of the input ligands. To avoid their abundant interpretation errors, output ligands should be checked for conservation of the 2D structure of the conformer predicting the lowest docking-score ADV docking-scores in Kcal/mol[54, 51, 55, 56] were converted to nM affinities by the formula, $10^{9}*(\exp^{(Kcal/mol/0.592)})$. A grid surrounding the whole ORF8 homodimer molecule of 45x45x45 Å was automatically centered around the PyMol / centerofmass. This grid size explored any other possible docking-cavities for each children, rather than those more limited by *DW-BEL* co-evolution.

Computational manipulations

Computational manipulation software and hardware were similar to those described in detail before. References are reproduced here for convenience:

Table 1
Software and hardware used here for computational manipulations

name	version	Main use	url
DataWarrior	Updated 5.5.0 Windows/Linus	Evolutionary docking[34] Commercial ChemSpace	https://openmolecules.org/ datawarrior/download.html)
Babel & AutoDockVina	Home-adapted PyRx 098/1.0	Force-field minimization & 2D conservation	https://pyrx.sourceforge.io/
MolSoft	3.9 Win64bit	Manipulation of sdf files	https://www.molsoft.com/download.html
PyMol	2.5.7.	Visualization of molecules	https://www.pymol.org/
Discovery Studio	21.1.1.0.20298	Visualization of molecules	https://discover.3ds.com/discovery-studio-visualizer-download
OriginPro	2022	Calculations and Figures	https://www.originlab.com/
LigPlot+	2.2.8.	Amino acid bonds of docked ligands	https://www.ebi.ac.uk/thornton--rv/software/LigPlus/applicence.html
AMD Ryzen i9 computer	4 DDR4 x 32 Gb memory	47 CPU Computational hardware	https://www.pcspecialist.es/

Results

Because there were no drugs approved for ORF8, probable best targets could be at its homodimer interface, as suggested [35]. Rather than targeting only the disulphide bond, we chose here a 45x45x45 Å grid (**Figure 3, left**) surrounding the ORF8 homodimer molecule (blind-docking) to search for any other alternative cavities. To start that search, we employed the *DW-BEL* co-evolution, because it generates tens of thousands children selecting those fitting nearby cavities from a parent molecule. Because we have no parent molecules, we designed from scratch a pseudoligand that we have called "erizo" (**Figure 1 up, red spheres** and **Figure 2 up-left**). The erizo was designed, optimized by several preliminary tests, manually drawn and docked to the center at the ORF8 homodimer (described in methods).

Wide enough to include the previously proposed disulfide target, the erizo co-evolutions rapidly began trimming, changing, adding and selecting erizo's atoms to generate a few thousands of children best fitting to any docking cavity located nearby those defined by the erizo. Using this strategy, only two docking cavities were repeatedly identified at the ORF8 homodimer. For instance, the co-evolution described here in more detail predicted 1409 fitting children. One of the cavities was located at the AB interface (53% of the children) and the other was located at its hypervariable A loop (**Figure 1, down**). Because of the hypervariable folds described for the A loop in previous crystallographic work, it was assumed that any of its possible ligands will be dependent on its particular protein interactions. Therefore, we focused these first studies on the AB interface.

.

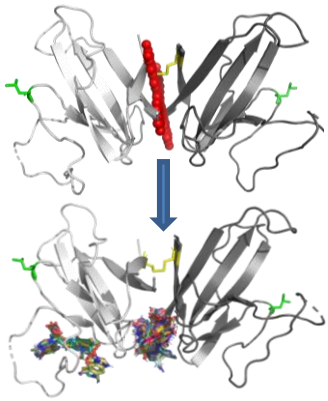

Figure 1
Erizo (up) and erizo's evolved top-children (down)
The ORF8 was targeted by *DW-BEL* co-evolution using the criteria described in methods to generate children from the erizo parent. The ADV docking was performed by blind-docking the erizo's children.
Gray cartoon, ORF8 asymmetric dimer chain A. **Darker gray cartoon**, ORF8 asymmetric dimer chain B
Yellow sticks, ^{20}C-^{20}C disulphide Cysteins between the A and B monomer chains of the ORF8 homodimer
Up red spheres, user-designed and manually docked "erizo" to start *DW-BEL* co-evolutions
Green sticks, amino acid positions of variants $L^{84}S$
Multicolor thin sticks, mapping of erizo's derived *DW-BEL* ADV first 100 top-children: docking to cavity A (left hypervariable loop at monomer A) and to cavity AB (interface of the asymmetrical homodimer).

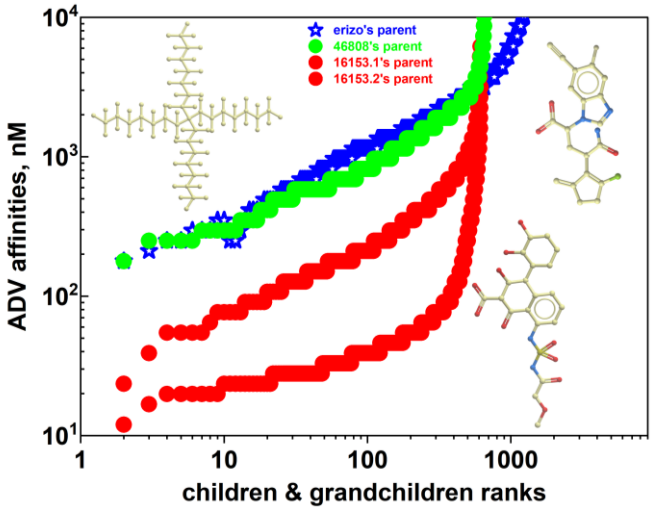

Figure 2
ADV affinity ranks of DW-BEL co-evolutions targeting the ORF8 AB cavity
2D geometries of the erizo (up-left) and the erizo's children 16153 and 46808 (right), were represented.
Blue open stars, erizo's parent co-evolution (3 runs generated 409 fitted-children)
Green closed circles, grandchildren from 46808 as parent (1 run generated 652 fitted-grandchildren)
Red closed circles, grandchildren from two independent runs from 16153 as parent (16153.1 generated 602, and 16153.2 generated 616 fitted-grandchildren, respectively)

ADV ranked erizo's children targeting the AB cavity according to their affinity predictions but there were none < 100 nM (**Figure 2**, **blue stars**). Two main scaffolds were repeated among all the generated children with some atom variations, including additions and changed atoms. To explore for possible higher affinities, two of their top-children were selected, each representing one different scaffold. Top-children numbers 16153 and 46808 representing each one of the scaffolds (**Figure 2, right** 2D geometries and **Table S2, children**), were selected to generate their corresponding grandchildren by additional *DW-BEL* co-evolution and ADV affinity ranking.

The corresponding results predicted many grandchildren with improved affinities compared to their parents only when they were generated from the 16153 children (Compare **Figure 2, red circles 1** with **Figure 2, green circles,** and **Table S2**, 16153 and 46808-derived grandchildren). Because of their random algorithms, to test whether their grandchildren ADV affinities could be incremented (lower docking-scores), additional *DW-BEL* co-evolutions were re-run using the 16153 children as parent. One of the additional runs tested, predicted grandchildren with higher ADV affinities (**Figure 2, red circles 2**). Furthermore, all of those grandchildren predicted a unique scaffold of 4 rings and the same docking cavity (**Figure 3, right**), despite the many other possibilities offered by the blind-docking grid (**Figure 3, left gray rectangle).** The first top-grandchildren was generated after 4670 grandchild (**Figure 3, right red**). In the case of grandchild 4670, one of its extreme rings predicted 2 Cl atoms and a short -CO-N-SO_2- link in between the 2 extreme rings (**Figure 4, right**). The main interactions between grandchild 4670 and the amino acids at the ORF8 homodimer interface, targeted ^{115}R at both A and B chains by two Hydrogen bonds (**Figure 4, left**), amino acids implicated in two salt bridges between A and B chains (^{119}D-^{115}R and ^{115}R-^{92}E, respectively). There were also other amino acids implicated in the homodimer interface that were targeted by 4670 such as those forming Hydrogen bonds to ^{94}K and ^{93}P as well as ^{120}F (Hydrogen bond ^{120}F-^{53}K). The predicted competition by two Hydrogen bonds with the ^{115}R homodimer two salt bridges, together with the rest of interactions may explain why the resulting nanoMolar affinities of 4670. Pending of experimental confirmation, those predicted interactions mentioned above and/or those of other of the top-grandchildren, could modify the natural conformation of the ORF8 homodimer interface.

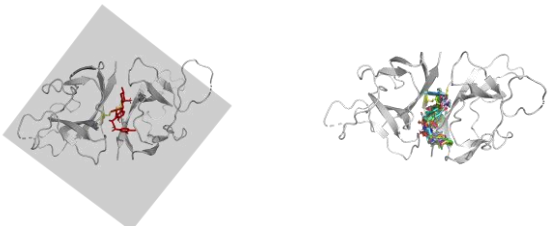

Figure 3
Bottom view of 4670 (left) and 33 other 16153 top-grandchildren (right) targeting the AB site
ORF8 homo dimer was ADV docked to top-grandchild 4670 or other 33 top-grandchildren.
Yellow sticks behind image, ^{20}C-^{20}C disulphide bond
Gray square background, 45x45x45 Å grid.
Grey cartoons, carbon backbone of the ORF8 asymmetric homodimer model
Red stick, first top-grandchild co-evolved from 16153.
Multi colour sticks, 15 top-grandchildren co-evolved from 16153

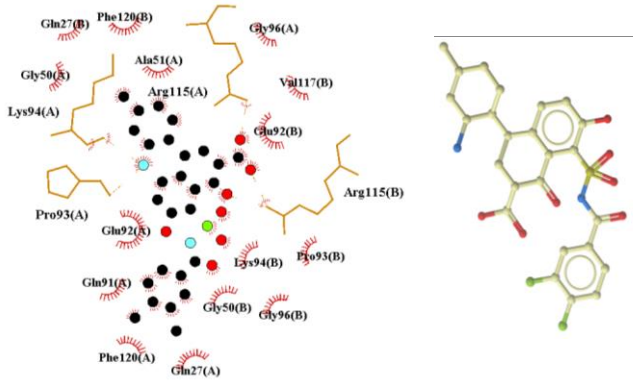

Figure 4
ADV docked 4670 top-child amino acids around 4 Å
The 4670-targeted amino acids in the ORF8 homodimer (Chains A and B) were described by their 3 letter code followed by their ORF8 chain in parenthesis.
Left) LigPlot predictions
Red circles, Oxygens. **Green circles**, Nitrogens. **Cyan circle**, Sulphur. **Black circles**, Carbons and Cl.
Brown sticks, ORF8 side-chains forming Hydrogen bonds (**brown hatched lines**, Hydrogen bonds).
Right) 4670 2D structure drawn at MolSoft.
Red circles, Oxygens. **Green circles**, Cl. **Blue circles**, Nitrogens. **Light green circle**, Sulphur.
Light green circles and sticks, Carbons and bonds

Discussion

Generation of children ligands by DW-BEL co-evolution and their affinity ranking by ADV blind-docking have been combined here to unrevealed some of the docking cavities at the ORF8 asymmetrical homodimer accessory SARS-COV-2 protein and to predict some novel putative ligands. Automatic rather than *a priori* selection by the programs, were preferred here to predict for new molecules with some possibilities to inhibit the interferences of ORF8 to the human immune response.

No ligand molecules were predicted around the disulphide link by blind-docking, most probably due to higher steric constrains. It was also surprising that **i)** the affinities predicted by the first round of co-evolutions were relatively low, at the 8-9 Kcal/mol ranges (similar to those predicted for hypothetical disulphide disruptors[35]) and **ii)** the numbers of grandchildren that could be generated from top-children (16153 or 46808), were in the hundreds rather than in the thousands, as usually expected . Thus, in our hands other *DW-BEL* co-evolutions generated thousands of fitted children with many different scaffolds[48, 58, 57, 58, 46]. In contrast, targeting ORF8 demanded higher computer memories, but only generated hundreds of grandchildren within unique or few scaffolds. The strong steric constrains of the highly interdigitated ORF8 interface may explain the difficulties experienced. Despite those difficulties, hundreds of unique grandchildren with no scaffold variations could successfully predict fitting their initial docking cavity.

The DW-BEL co-evolutions applied in this work have benefit from several improvements that have been incorporated step-by-step during the last months to their algorithms by studying the targeting characteristics of different protein / ligand models [48, 58, 57, 58, 46]. However, it seems likely that the continuation of such explorations with probability to find more alternatives, would demand higher computer memories to penetrate further in the vast chemical space[38, 39]. In particular, to overcome the steric difficulties to find out additional molecules predicting high affinity insertions into the narrow space between the A and B ORF8 faces, computers with more speed and memories would be required.

Apart from the hypothetical pseudoligand used here to start co-evolutions, other limitations may also include the fixed docking-cavities. Considering the influences of the side-chain mobilities on docking affinity estimations may add small variations to best accommodate any of the predicted ligands. However, their higher memory demands would made the explorations of those possibilities difficult to apply to high numbers of children molecules. Alternatively, other more adaptable ORF8 docking cavities may still exist such as those in: **i)** the interface of the hypervariable loop A with another ORF8 monomer as it was earlier suggested by their surface complementarity in crystallographic models[36] or with **ii**) some of the many protein molecular surfaces of human proteins with already demonstrated interactions with ORF8 and/or those that have been computationally predicted by interactome studies. Further computational work could further clarify these hypothetical alternatives.

Supporting information

Table S1
***Special SD-File* save options to conserve 2D geometries of *DW-BEL* children during ADV**

Save special options	**1**	**2**
Structure column	Docked protonation state	Structure
SD-file version	Version 3	Version 3
Atom coordinates	Docking pose	3D (1st of multiple)
□ Include.....	Cavity & Natural Ligand	RefCompound
Compound name column	ID	ID
2D geometry conservation	MAXIMAL	MINIMAL

Table S2
Molecular properties of selected children and some of their representative first top-grandchildren

			ADV		DW
ID	**MW**	**cLogP**	**Kcal/mol**	**nM**	**score**
16153	486	-0.9	-8.9	295.1	-79.8
4670	568	2.0	-10.6	16.7	-98.5
4975	546	1.7	-10.4	23.4	-97.7
4625	566	1.9	-10.3	27.7	-107.0
5943	516	0.8	-10.3	27.7	-101.6
6413	536	1.1	-10.3	27.7	-98.5
1706	519	1.1	-10.2	32.9	-95.8
46808	401	1.9	-9.0	249.5	-84.7
3956	540	2.1	-9.2	178.2	-113.0
1513	421	3.0	-8.9	295.7	-92.3
5700	549	2.6	-8.9	295.7	-107.8
1833	433	2.9	-8.8	350.2	-93.3
5122	520	1.8	-8.8	350.2	-112.6

Supporting Materials included in the **33top-grandchildren.*dwar***. file contained *DW* tables with 33 top-grandchildren selected by the **dw-adv2.py macro** selected grandchildren predicting < -95 DW docking-scores and - 10 Kcal/mol ADV docking-scores. Tables are provided with threshold *slider-filters* to their *DW* and ADV docking-scores, *Molecular weights* and *clogP* properties to select particular threshold combinations.

Supporting Materials

- NTNV.dwam. A *.dwam file *DW* macro developed to save, label and eliminate any children molecules generated during *DW-BEL* co-evolution which contained any known *T*oxicity risks (*Mutagenesis, Tumorigenicity, Reproductive Interference, Irritant*) and/or any of the numerous *Nasty Functions* (see **Nasty_functions.dwar**). The macro uses *.sdf or *.*dwar* files as inputs, user-renamed the input *.*dwar* file and renamed and saved the corresponding *.sdf file. This saving method supplied *.sdf files maintaining the 3D protein cavity docked to children 3D conformers for visualization in PyMol (using its split_states command) and/or maximal preservation of their 2D geometries for optimal consensus docking (**Table S1**). More than ~ 3000 traded drugs were taken by *DW* as low toxicity reference (https://github.com/thsa/datawarrior/blob/master/src/html/properties/properties.html. Additional information on the *DW Toxicity* risks evaluated can be found at the **R**egistry of **T**oxic **E**ffects of **C**hemical **S**ubstances (RTECS data base) (https://www.cdc.gov/niosh/docs/97-119/default.html).

- ***Nasty_functions.dwar.*** List of previously defined *DW Nasty functions* of small chemical fragments having known physiological interference problems, kindly supplied by Dr.T.Sander of *DW* (https://openmolecules.org/forum/index.php?t=msg&th=662&start=0&).

- **dw-adv2.py**. Python macro user-developed to select for the consensus top-children according to user-defined combinations of *DW-BEL* and ADV docking-score predictions contained in *.sdf files.

- **33top-grandchildren.*dwar***. These *.dwar *DW* tables contain 33 top-grandchildren selected by the **dw-adv2.py macro** for grandchildre predicting < -95 DW docking-scores and - 10 Kcal/mol ADV docking-scores. Tables are provided with threshold *slider-filters* to their *DW* and ADV docking-scores, *Molecular weights* and *clogP* properties to select particular threshold combinations. The *.*dwar* files can be opened in *DW* https://openmolecules.org/datawarrior/download.htm.

- **33top-grandchildren.pse**. The 33 top-grandchildren ADV complexes with the ORF8 asymmetrical homodimer crystalographic 7jtl model to be visualized in PyMol vs2.5.3. (**Figure S3**).

Funding
The work was carried out without any external financial contribution

Competing interests
The author declares no competing interests

Authors' contributions
JC designed, performed and analyzed the dockings and drafted the manuscript.

Acknowledgements
Thanks are specially due to N.Berndt of Idorsia Pharmaceuticals Ltd. at Allschwil (Switzerland) for help to develop the NTN DW macro and discussions on the DW forum. Thanks are also due to Dr. A. Villena from the University of Leon (Spain) for advise.

References

[1]Takatsuka, H., *et al.* In silico Analysis of SARS-CoV-2 ORF8-Binding Proteins Reveals the Involvement of ORF8 in Acquired-Immune and Innate-Immune Systems.*Front Med (Lausanne).* 2022, 9: 824622 1http://dx.doi.org/0.3389/fmed.2022.824622.

[2]Arduini, A., *et al.* SARS-CoV-2 ORF8: A Rapidly Evolving Immune and Viral Modulator in COVID-19.*Viruses.* 2023, 15: http://dx.doi.org/10.3390/v15040871.

[3]Hassan, S.S., *et al.* A unique view of SARS-CoV-2 through the lens of ORF8 protein.*Comput Biol Med.* 2021, 133: 104380 http://dx.doi.org/10.1016/j.compbiomed.2021.104380.

[4]Kohyama, M., *et al.* SARS-CoV-2 ORF8 is a viral cytokine regulating immune responses.*Int Immunol.* 2023, 35: 43-52 http://dx.doi.org/10.1093/intimm/dxac044.

[5]Zinzula, L. Lost in deletion: The enigmatic ORF8 protein of SARS-CoV-2.*Biochem Biophys Res Commun.* 2021, 538: 116-124 http://dx.doi.org/10.1016/j.bbrc.2020.10.045.

[6]Akaishi, T., *et al.* Insertion/deletion hotspots in the Nsp2, Nsp3, S1, and ORF8 genes of SARS-related coronaviruses.*BMC Ecol Evol.* 2022, 22: 123 http://dx.doi.org/10.1186/s12862-022-02078-7.

[7]Twohig, K.A., *et al.* Hospital admission and emergency care attendance risk for SARS-CoV-2 delta (B.1.617.2) compared with alpha (B.1.1.7) variants of concern: a cohort study.*Lancet Infect Dis.* 2022, 22: 35-42 http://dx.doi.org/10.1016/S1473-3099(21)00475-8.

[8]Young, B.E., *et al.* Effects of a major deletion in the SARS-CoV-2 genome on the severity of infection and the inflammatory response: an observational cohort study.*Lancet.* 2020, 396: 603-611 http://dx.doi.org/10.1016/S0140-6736(20)31757-8.

[9]Hassan, S.S., *et al.* An issue of concern: unique truncated ORF8 protein variants of SARS-CoV-2.*PeerJ.* 2022, 10: e13136 http://dx.doi.org/10.7717/peerj.13136.

[10]Bykova, A., *et al.* The 29-nucleotide deletion in SARS-CoV: truncated versions of ORF8 are under purifying selection.*BMC Genomics.* 2023, 24: 387 http://dx.doi.org/10.1186/s12864-023-09482-3.

[11]Brandt, D., *et al.* Multiple Occurrences of a 168-Nucleotide Deletion in SARS-CoV-2 ORF8, Unnoticed by Standard Amplicon Sequencing and Variant Calling Pipelines.*Viruses.* 2021, 13: http://dx.doi.org/10.3390/v13091870.

[12]DeRonde, S., *et al.* Identification of a Novel SARS-CoV-2 Strain with Truncated Protein in ORF8 Gene by Next Generation Sequencing.*Res Sq.* 2021: http://dx.doi.org/10.21203/rs.3.rs-413141/v1.

[13]Vinjamuri, S., *et al.* SARS-CoV-2 ORF8: One protein, seemingly one structure, and many functions.*Front Immunol.* 2022, 13: 1035559 http://dx.doi.org/10.3389/fimmu.2022.1035559.

[14]Sadegh, S., *et al.* Exploring the SARS-CoV-2 virus-host-drug interactome for drug repurposing.*Nat Commun.* 2020, 11: 3518 http://dx.doi.org/10.1038/s41467-020-17189-2.

[15]Messina, F., *et al.* COVID-19: viral-host interactome analyzed by network based-approach model to study pathogenesis of SARS-CoV-2 infection.*J Transl Med.* 2020, 18: 233 http://dx.doi.org/10.1186/s12967-020-02405-w.

[16]Liu, P., *et al.* SARS-CoV-2 ORF8 reshapes the ER through forming mixed disulfides with ER oxidoreductases.*Redox Biol.* 2022, 54: 102388 http://dx.doi.org/10.1016/j.redox.2022.102388.

[17]Rashid, F., *et al.* The ORF8 protein of SARS-CoV-2 induced endoplasmic reticulum stress and mediated immune evasion by antagonizing production of interferon beta.*Virus Res.* 2021, 296: 198350 http://dx.doi.org/10.1016/j.virusres.2021.198350.

[18]Wang, X., *et al.* SARS-CoV-2 ORF8 Protein Induces Endoplasmic Reticulum Stress-like Responses and Facilitates Virus Replication by Triggering Calnexin: an Unbiased Study.*J Virol.* 2023, 97: e0001123 http://dx.doi.org/10.1128/jvi.00011-23.

[19]Lehrer, S. and Rheinstein, P.H. Alignment of human KAT2A (GCN5) histone acetyltransferase and SARS-CoV-2 Orf8 viral proteins.*Chronic Dis Transl Med.* 2022, 9: 263-5 http://dx.doi.org/10.1002/cdt3.56.

[20]Chou, J.M., *et al.* The ORF8 Protein of SARS-CoV-2 Modulates the Spike Protein and Its Implications in Viral Transmission.*Front Microbiol.* 2022, 13: 883597 http://dx.doi.org/10.3389/fmicb.2022.883597.

[21]Hussain, M., *et al.* Immunoinformatic analysis of structural and epitope variations in the spike and Orf8 proteins of SARS-CoV-2/B.1.1.7.*J Med Virol.* 2021, 93: 4461-4468 10.1002/jmv.26931.

[22]Kim, I.J., *et al.* SARS-CoV-2 protein ORF8 limits expression levels of Spike antigen and facilitates immune evasion of infected host cells.*J Biol Chem.* 2023, 299: 104955 http://dx.doi.org/10.1016/j.jbc.2023.104955.

[23]Kumar, J., *et al.* SARS-CoV-2-encoded ORF8 protein possesses complement inhibitory properties.*J Biol Chem.* 2023, 299: 102930 http://dx.doi.org/10.1016/j.jbc.2023.102930.

[24]Fernandes, M.F., *et al.* Effect of cannabidiol on apoptosis and cellular interferon and interferon-stimulated gene responses to the SARS-CoV-2 genes ORF8, ORF10 and M protein.*Life Sci.* 2022, 301: 120624 http://dx.doi.org/10.1016/j.lfs.2022.120624.

[25]Chen, J., *et al.* Severe Acute Respiratory Syndrome Coronavirus 2 ORF8 Protein Inhibits Type I Interferon Production by Targeting HSP90B1 Signaling.*Front Cell Infect Microbiol.* 2022, 12: 899546 http://dx.doi.org/10.3389/fcimb.2022.899546.

[26]Geng, H., *et al.* SARS-CoV-2 ORF8 Forms Intracellular Aggregates and Inhibits IFNgamma-Induced Antiviral Gene Expression in Human Lung Epithelial Cells.*Front Immunol.* 2021, 12: 679482 http://dx.doi.org/10.3389/fimmu.2021.679482.

[27]Li, J.Y., *et al.* The ORF6, ORF8 and nucleocapsid proteins of SARS-CoV-2 inhibit type I interferon signaling pathway.*Virus Res.* 2020, 286: 198074 http://dx.doi.org/10.1016/j.virusres.2020.198074.

[28]Hamdorf, M., *et al.* The unique ORF8 protein from SARS-CoV-2 binds to human dendritic cells and induces a hyper-inflammatory cytokine storm.*J Mol Cell Biol.* 2023: http://dx.doi.org/10.1093/jmcb/mjad062.

[29]Lin, X., *et al.* Unconventional secretion of unglycosylated ORF8 is critical for the cytokine storm during SARS-CoV-2 infection.*PLoS Pathog.* 2023, 19: e1011128 http://dx.doi.org/10.1371/journal.ppat.1011128.

[30]Wu, X., *et al.* Viral Mimicry of Interleukin-17A by SARS-CoV-2 ORF8.*mBio.* 2022, 13: e0040222 http://dx.doi.org/10.1128/mbio.00402-22.

[31]Beaudoin-Bussieres, G., *et al.* SARS-CoV-2 Accessory Protein ORF8 Decreases Antibody-Dependent Cellular Cytotoxicity.*Viruses.* 2022, 14: http://dx.doi.org/10.3390/v14061237.

[32]Wu, X., *et al.* Secreted ORF8 induces monocytic pro-inflammatory cytokines through NLRP3 pathways in patients with severe COVID-19.*iScience.* 2023, 26: 106929 http://dx.doi.org/10.1016/j.isci.2023.106929.

[33]Zhang, Y., *et al.* The ORF8 protein of SARS-CoV-2 mediates immune evasion through down-regulating MHC-Iota.*Proc Natl Acad Sci U S A.* 2021, 118: http://dx.doi.org/10.1073/pnas.2024202118.

[34]Chaudhari, A.M., *et al.* Defective ORF8 dimerization in SARS-CoV-2 delta variant leads to a better adaptive immune response due to abrogation of ORF8-MHC1 interaction.*Mol Divers.* 2023, 27: 45-57 http://dx.doi.org/10.1007/s11030-022-10405-9.

[35]Selvaraj, C., *et al.* SARS-CoV-2 ORF8 dimerization and binding mode analysis with class I MHC: computational approaches to identify COVID-19 inhibitors.*Brief Funct Genomics.* 2023, 22: 227-240 http://dx.doi.org/10.1093/bfgp/elac046.

[36]Flower, T.G., *et al.* Structure of SARS-CoV-2 ORF8, a rapidly evolving immune evasion protein.*Proc Natl Acad Sci U S A.* 2021, 118: http://dx.doi.org/10.1073/pnas.2021785118.

[37]Cheng, Y. and Peng, X. In silico study on the effects of disulfide bonds in ORF8 of SARS-CoV-2.*Phys Chem Chem Phys.* 2022, 24: 16876-16883 http://dx.doi.org/10.1039/d2cp01724e.

[38]Wu, F., *et al.* Glycosylated, Lipid-Binding, CDR-Like Domains of SARS-CoV-2 ORF8 Indicate Unique Sites of Immune Regulation.*Microbiol Spectr.* 2023, 11: e0123423 http://dx.doi.org/10.1128/spectrum.01234-23.

[39]Pereira, F. Evolutionary dynamics of the SARS-CoV-2 ORF8 accessory gene.*Infect Genet Evol.* 2020, 85: 104525 http://dx.doi.org/10.1016/j.meegid.2020.104525.

[40]Laha, S., *et al.* Characterizations of SARS-CoV-2 mutational profile, spike protein stability and viral transmission.*Infect Genet Evol.* 2020, 85: 104445 http://dx.doi.org/10.1016/j.meegid.2020.104445.

[41]Islam, S., *et al.* Structural and functional effects of the L84S mutant in the SARS-COV-2 ORF8 dimer based on microsecond molecular dynamics study.*J Biomol Struct Dyn.* 2023: 1-18 http://dx.doi.org/10.1080/07391102.2023.2228919.

[42]Matsuoka, K., *et al.* SARS-CoV-2 accessory protein ORF8 is secreted extracellularly as a glycoprotein homodimer.*J Biol Chem.* 2022, 298: 101724 http://dx.doi.org/10.1016/j.jbc.2022.101724.

[43]Lin, X., *et al.* ORF8 contributes to cytokine storm during SARS-CoV-2 infection by activating IL-17 pathway.*iScience.* 2021, 24: 102293 http://dx.doi.org/10.1016/j.isci.2021.102293.

[44]Hachim, A., *et al.* ORF8 and ORF3b antibodies are accurate serological markers of early and late SARS-CoV-2 infection.*Nat Immunol.* 2020, 21: 1293-1301 http://dx.doi.org/10.1038/s41590-020-0773-7.

[45]Chen, X., *et al.* Crystal Structures of Bat and Human Coronavirus ORF8 Protein Ig-Like Domain Provide Insights Into the Diversity of Immune Responses.*Front Immunol.* 2021, 12: 807134 http://dx.doi.org/10.3389/fimmu.2021.807134.

[46]Coll, J.M. Exploring non-toxic co-evolutionary docking.*ChemRxiv.* 2023: https://chemrxiv.org/engage/chemrxiv/article-details/6512b162ade1178b2424c325.

[47]Bryant, P., *et al.* Structure prediction of protein-ligand complexes from seqeunce information with Umol.*bioRxiv.* 2023: https://doi.org/10.1101/2023.11.03.565471.

[48]Coll, J.M. Evolutionary-docking targeting bacterial FtsZ.*ChemRxiv.* 2023: https://chemrxiv.org/engage/chemrxiv/article-details/6405c36fcc600523a3bcb679.

[49]Wahl, J., *et al.* Accuracy evaluation and addition of improved dihedral parameters for the MMFF94s.*J Cheminform.* 2019, 11: 53 http://dx.doi.org/10.1186/s13321-019-0371-6.

[50]Coll, J. Star-shaped Triazine-derivatives: would they crossbind SARS-CoV-2 spike helices?*ChemRxiv.* 2021, https://chemrxiv.org/engage/chemrxiv/article-details/6133c1096563696d9d222bbd: http://dx.doi.org/10.33774/chemrxiv-2021-xb6sx-v2.

[51]Lorenzo, M.M., *et al.* Would it be possible to stabilize prefusion SARS-COV-2 spikes with ligands?*ChemRxiv.* 2021: http://dx.doi.org/10.26434/chemrxiv.13453919.v2.

[52]Bermejo-Nogales, A., *et al.* Computational ligands to VKORC1s and CYPs. Could they predict new anticoagulant rodenticides?*BioRxiv.* 2021: http://dx.doi.org/10.1101/2021.01.22.426921.

[53]Dallakyan, S. and Olson, A.J. Small-molecule library screening by docking with PyRx.*Methods Mol Biol.* 2015, 1263: 243-50 http://dx.doi.org/10.1007/978-1-4939-2269-7_19.

[54]Morris, G.M., *et al.* AutoDock4 and AutoDockTools4: Automated docking with selective receptor flexibility.*J Comput Chem.* 2009, 30: 2785-91 http://dx.doi.org/10.1002/jcc.21256.

[55]Huey, R., *et al.* A semiempirical free energy force field with charge-based desolvation.*J Comput Chem.* 2007, 28: 1145-52 http://dx.doi.org/10.1002/jcc.20634.

[56]Trott, O. and Olson, A.J. AutoDock Vina: improving the speed and accuracy of docking with a new scoring function, efficient optimization, and multithreading.*J Comput Chem.* 2010, 31: 455-61 http://dx.doi.org/10.1002/jcc.21334.

[57]Coll, J.M. Anticoagulant rodenticide novel candidates predicted by evolutionary docking.*ChemRxiv.* 2023: https://chemrxiv.org/engage/chemrxiv/article-details/6479b8cfbe16ad5c57577cce.

[58]Coll, J. Could Acinetobacter baumannii LoI-abaucin docking be improved?*ChemRxiv.* 2023: https://chemrxiv.org/engage/chemrxiv/article-details/649aa71aba3e99daef1d1756.